Coupled Processes and the Tropical Climatology. Part III: Instabilities of the Fully Coupled Climatology*

HENK A. DIJKSTRA

Institute for Marine and Atmospheric Research Utrecht, Utrecht University, Utrecht, the Netherlands

J. DAVID NEELIN

Department of Atmospheric Sciences and Institute of Geophysics and Planetary Physics, University of California, Los Angeles, Los Angeles, California

(Manuscript received 24 October 1997, in final form 23 June 1998)

ABSTRACT

Coupled processes between the equatorial ocean and atmosphere control the spatial structure of the annual-mean state in the Pacific region, in particular the warm pool–cold tongue structure. At the same time, coupled processes are known to be responsible for the variability about this mean state, in particular the El Niño–Southern Oscillation phenomenon. In this paper, the connection between both effects of coupling is considered by investigating the linear stability of fully coupled climatologies in an intermediate coupled model. The new element here is that when parameters—such as the coupling strength—are changed, the potential amplification of disturbances can be greatly influenced by a simultaneous modification of the mean state. This alters the stability properties of the coupled climatology, relative to the flux-corrected cases that have been previously studied. It appears possible to identify a regime in parameter space where ENSO-like unstable modes coincide with a reasonable warm pool–cold tongue structure. These unstable modes are mixed SST–ocean dynamics modes, that is, they arise through an interaction of oscillatory modes originating from ocean dynamics and oscillatory SST modes. These effects are qualitatively similar in this fully coupled problem compared to the flux-corrected problem, but the sensitivity of the ENSO mode to parameters and external variations is larger due to feedbacks in the climatology.

1. Introduction

Interaction of the tropical atmosphere and the Pacific Ocean causes one of the dominant sources of interannual variability in the climate system, the El Niño–Southern Oscillation (ENSO) phenomenon (see Philander 1990). In current theory, ENSO arises as a self-sustained cycle in which anomalies of SST cause the trade winds to strengthen and weaken. This drives changes in ocean circulation that produce anomalous SST; the memory of this cycle is provided by adjustment processes in the ocean (see, e.g., Schopf and Suarez 1988, 1990; Battisti and Hirst 1989; Philander 1990; Neelin et al. 1994 and references therein).

Linear stability analyses of idealized annual-mean states in intermediate coupled models have provided much of our understanding of how large-scale coupled feedbacks give rise to an oscillatory unstable ENSO mode. One of the models that is believed to capture much of the essential physics of the coupled system is that of Zebiak and Cane (1987), referred to below as the ZC model. For a spatially constant climatology, the most unstable modes were determined by Hirst (1986) in a simplified ZC-like model with periodic conditions at the east–west ocean boundaries. Hirst (1986) focuses on coupled long wavelength traveling waves, which can become unstable at strong enough coupling, that are related to oceanic long Rossby and Kelvin waves. Hirst (1986) mentions that a third class of traveling waves—related to the evolution of the sea surface temperature (SST)—is possible. Neelin (1991) termed these SST modes, and discussed the strong role of coupling in creating them.

The same stability problem has been considered within ZC-type models within a finite ocean basin in a number of studies (Hirst 1988; Wakata and Sarachik 1991; Jin and Neelin 1993a,b; Neelin and Jin 1993). In all of these, the mean state has been constructed by using observed (or idealized prescribed) surface winds to

* Institute of Geophysics and Planetary Physics Contribution Number 4889.

Corresponding author address: Dr. Henk A. Dijkstra, Inst. for Marine and Atmospheric Research Utrecht, Utrecht University, 3508TA Utrecht, the Netherlands.
E-mail: dijkstra@phys.uu.nl

© 1999 American Meteorological Society

Unauthenticated | Downloaded 07/18/24 11:00 AM UTC

compute the mean response of the ocean, within a procedure known as ''flux correction.'' In these models, the atmosphere response is considered only on the perturbations of this mean state. For these flux-corrected mean states, a unified view of all the relevant modes was presented in a three part study by Jin and Neelin (1993a,b) and Neelin and Jin (1993) (collectively JN hereafter). For the ''stripped down'' version of the ZC model used by JN, two classes of oscillatory coupled modes appear. The first class of oscillatory instabilities originates from ocean wave dynamics and is the counterpart of the traveling wave modes in the periodic basin. The spectrum of the ocean dynamics modes is complicated because it is basically continuous and discretization of the operator leaves a resolution-dependent spectrum, the ''scattering spectrum.'' The second class of oscillatory modes are SST modes and these modes may become stationary in some parameter regimes. In the fast wave limit, these stationary instabilities were shown to be related to transcritical bifurcations leading to multiple stable equilibria (Hao et al. 1993; Dijkstra and Neelin 1995a). In certain limits (e.g., the fast-wave and fast-SST limits) these modes are separated but in the realistic area in parameter space, the eigenmodes are of mixed SST–ocean dynamics type. Jin and Neelin (1993a) showed that eigensurfaces spanned by both type of modes are continuously connected in parameter space. In the realistic regime, the climatology is unstable to oscillatory modes of which the spatial structure is set by an SST mode, while the internal frequency is determined largely by subsurface memory through ocean adjustment.

The mixed SST–ocean dynamics mode interpretation of the ENSO mode incorporates the subsurface memory paradigm known as the SSBH delayed oscillator model (Schopf and Suarez 1988; Suarez and Schopf 1988; Battisti and Hirst 1989). In JN it is shown how the SSBH delayed oscillator model captures a particular regime of the mixed SST–ocean dynamics modes, while the Cane et al. (1990) and Münnich et al. (1991) mode captures a related regime. Jin (1997a,b) proposed an even simpler model, termed a ''recharge oscillator,'' that captures in the fewest possible degrees of freedom the mixed nature of the ENSO mode. In all these models, the subsurface heat content carries the oscillation through a transition phase where the SST anomaly in the eastern Pacific is nearly zero. The disequilibrium between thermocline anomalies and wind stress anomalies drives the cycle. On the equator the symptom of this is that western Pacific heat content leads eastern Pacific heat content by between 90° and 180° of temporal phase.

The picture that has emerged from the previous studies is that some mean state becomes unstable at sufficiently large coupling strength. Oscillatory disturbances are amplified through coupled feedbacks and give way to a sustained oscillation. In mathematical terms, the dynamical system becomes unstable through a forward Hopf bifurcation and a limit cycle emerges with an internal frequency set by the eigenvalues at the bifurcation. It is this internal frequency that lies at the heart of the ENSO cycle, since it also determines to a large extent the phase locking to the annual cycle and the overlapping resonances that can lead to ENSO chaos (Jin et al. 1994, 1996; Tziperman et al. 1994, 1995; Chang et al. 1994, 1995).

Strong support for the conjecture that coupled processes also substantially determine the climatology in the tropical Pacific was given in the first two parts of this paper (Neelin and Dijkstra 1995; Dijkstra and Neelin 1995b), referred to below as ND and DN, respectively. An external wind stress, arising by factors outside the Pacific basin, causes a small zonal SST gradient and is amplified and modified by coupled feedbacks. In ND, it was shown that stationary instabilities from a flux-corrected climatology are not robust as the flux correction is relaxed to a fully coupled case. An imperfection of the system occurs, whereby a topological change in the branches of steady states occurs; the transcritical bifurcation is broken and two separate branches of steady states appear. One branch is continuously ''deformed'' to the climatology of the fully coupled case; the other branch disappears. Multiple equilibria that occur in the flux-corrected case are spurious by-products of the flux correction affecting physical feedbacks. This justifies the focus on oscillatory instabilities, rather than on stationary ones, of the flux-corrected mean states although the latter can be useful in understanding the origin of these oscillatory modes.

It was further shown in Dijkstra and Neelin (1995b) that a reasonable warm pool–cold tongue climatology can be obtained through coupled feedbacks acting on a ''seed'' SST field generated by the external wind stress, provided the magnitude of the latter is not too small. The size of the external wind stress must give sufficient external upwelling for the ensuing coupled feedbacks to create the correct spatial pattern and to set the amplitude of the cold tongue. Because of the importance of coupled feedbacks, the mean state itself will change as the parameters are changed that control the feedbacks. Sun and Liu (1996), Jin (1996), Liu (1997), and Liu and Huang (1997) further explored the role of coupling in the Walker circulation and associated SST gradients. Cane et al. (1997) examined such feedbacks applied to a global warming scenario. Examination of a related role of coupling in latitudinal asymmetries about the equator has been carried out by Xie (1994, 1996), Xie and Philander (1994), and Philander et al. (1996).

To unify the origin of the spatial structure of the mean state with the origin of its interannual oscillatory instabilities, both determined by coupled feedbacks, is one of the challenges in understanding the tropical climate system. Jin (1996) considered these issues using a simple box model of the coupled system and found ENSO-like instabilities on a simple mean state with reasonable east–west SST difference. The same problem is considered in this paper, but using the intermediate model

Unauthenticated | Downloaded 07/18/24 11:00 AM UTC

considered in DN. This captures much more of the spatio-temporal structure than the box model of Jin (1996).

Again, continuation methods appear to be a very efficient tool for following branches of fully coupled climatologies in parameter space, together with an eigenvalue curve of the linear stability problem. It will be shown that there exists at least one parameter regime where unstable ENSO-like modes coincide with a correct spatial structure of the mean state. The mean state is generated by the coupled processes as explained in DN. Connections of the coupled modes are followed through various parameter regimes to compare their origin to results known from previous studies of the flux-corrected case. Simultaneous sensitivity of the ENSO mode and the coupled climatology is then examined.

2. Formulation

a. Model

Following our earlier work, we consider an intermediate coupled equatorial ocean–atmosphere model consisting of a shallow water layer of mean depth H with an embedded mixed layer of fixed depth H_1 in an ocean basin of length L. This ocean model is coupled to a Gill (Gill 1980) atmosphere model; we keep the notation as in earlier papers (e.g., DN) unless otherwise specified. The temperature, horizontal and vertical velocities, time, and thermocline depth are scaled with a characteristic temperature difference ΔT, the oceanic Kelvin wave speed c_0, c_0H/L, L/c_0, and H, respectively. The nondimensional SST equation of the coupled model is then given by

$$\frac{\partial T}{\partial t} + u_1\frac{\partial T}{\partial x} + \mathcal{H}(w_1)w_1[T - T_s(h)] - \mathcal{H}(-v_N)v_N(T - T_N) + \epsilon_T(T - T_0) = 0, \quad (1)$$

where u_1 is the zonal velocity in the mixed layer, w_1 the vertical velocity just below the mixed layer, T_0 the radiation equilibrium temperature, and T_N is a fixed off-equatorial temperature. Moreover, ϵ_T is a constant representing Newtonian cooling by surface fluxes and $\mathcal{H}$ is the Heaviside function. The off-equatorial meridional velocity v_N follows from a discretization of the continuity equation (Neelin 1991). The subsurface temperature $T_s(h)$ depends on h according to

$$T_s(h) = T_{so} + (T_0 - T_{so})\tanh(\eta_1 h + \eta_2), \quad (2)$$

with $\eta_1 = H/H_*$, $\eta_2 = h_0/H_*$ and where h_0 and H_* control the steepness and the offset of the T_s profile and T_{so} is the characteristic temperature being upwelled into the surface layer.

The mean horizontal velocities u, v and the thermocline depth h satisfy long-wave shallow water dynamics, which, in dimensionless variables, become

$$\begin{aligned} \delta u_t + ru - yv + h_x &= \tau^x \\ yu + h_y &= 0 \\ \delta h_t + rh + u_x + v_y &= 0. \end{aligned} \quad (3)$$

In these equations, r is the oceanic damping (Rayleigh friction) coefficient. The parameter δ measures the ratio of the timescale of adjustment by oceanic dynamics to the timescale of SST change. Furthermore, τ^x is the zonal wind stress and the meridional wind stress is negelcted. The zonal velocity vanishes at the eastern boundary and a zero mass flux condition is applied at the western boundary; all quantities are bounded far from the equator.

As in DN, the zonal wind stress forcing τ^x is decomposed into

$$\tau^x = [\tau_{\text{ext}} + \mu A(T - T_0)]e^{-(1/2)\alpha y^2}. \quad (4a)$$

The wind stress part indicated by τ_{ext} is considered to originate from factors outside of the basin as thoroughly discussed in ND. The quantity μ is the coupling strength and the parameter α is the ratio of Rossby deformation radii in ocean and atmosphere. The atmosphere model operator A from the Gill model, representing the equatorial surface zonal wind, is given by

$$A(T; x, t) = \frac{3}{2}\exp(3\epsilon_a x)\int_x^1 \exp(-3\epsilon_a s)T(s, t)\,ds - \frac{1}{2}\exp(-\epsilon_a x)\int_0^x \exp(\epsilon_a s)T(s, t)\,ds, \quad (4b)$$

where ϵ_a is the dimensionless damping coefficient. The mixed layer velocities u_1 and w_1 follow from

$$u_1 = u_s + u; \qquad w_1 = w_s + w, \quad (5a)$$

where the subscript s indicates the surface layer velocities induced by Ekman dynamics. These are parameterized as in Neelin (1991), and in DN, for example, the vertical equatorial surface velocity is given by

$$w_s = -[\delta_F\tau_{\text{ext}} + \mu\delta_s A(T - T_0)], \quad (5b)$$

where δ_F measures the strength of the external upwelling and δ_s measures the strength of the surface layer feedback. This model setup is very similar to that used in Jin and Neelin (1993a), which considered the stability of flux-corrected climatologies.

b. Steady states and linear stability

To be compatible with the steady states computed in Parts I and II (ND, DN), zonal advection, oceanic damping, and the meridional extension of the wind field are neglected in the computation of the steady-state climatology, although they are included for the calculation of the time-dependent modes. This has little impact on the steady state and speeds up the computation. More explicitly, the basic states $\overline{T}$, $\overline{h}$, and $\overline{A}$ are determined from

Unauthenticated | Downloaded 07/18/24 11:00 AM UTC

$$\mathcal{H}(\overline{w}_1)\overline{w}_1[\overline{T} - T_s(\overline{h})] - \mathcal{H}(-\overline{v}_N)\overline{v}_N(\overline{T} - T_N) + \epsilon_T(\overline{T} - T_0) = 0. \quad (6)$$

The steady thermocline field $\overline{h}$ is determined from the steady shallow water equations (3) with zero damping ($r = 0$) and with $\alpha = 0$ in (4a). For these steady states the mean vertical velocity w is zero and hence $\overline{w}_1 = \overline{w}_s$.

As in DN, $\tau_{\text{ext}} = \overline{\tau}_z$ is taken to be zonally constant with small amplitude such that a weak zonal SST gradient appears for $\mu = 0$. As μ is increased, realistic cold tongue–warm pool configurations are obtained in some areas of parameter space. Note that the climatology thus obtained varies with control parameters, for example, the coupling strength μ, contrary to the flux-corrected case considered in JN, where the climatology is a solution for all values of μ. This implies that the calculation of the linear stability cannot be separated from that of its basic state.

In the linear stability problem for a particular steady state $(\overline{A}, \overline{T}, \overline{h})$ the evolution of infinitesimally small perturbations $(\hat{A}, \hat{T}, \hat{h})$ is considered. Linearization of the full SST equation around this steady state leads to

$$\frac{\partial \hat{T}}{\partial t} + a_T\hat{T} - a_h\hat{h} + a_w\hat{w}_1 + a_v\hat{v}_N + a_u\hat{u} = 0, \quad (7)$$

where the coefficients a (for expressions, see appendix A) are all spatially varying and $\hat{w}_1$, $\hat{v}_N$ can both be expressed into $\hat{h}$ and $\hat{A}$. In a normal mode analysis, solutions of the form

$$\hat{T}(x, t) = e^{\sigma t}\tilde{T}(x) \quad (8)$$

are sought, with similar dependencies for the other dependent quantities. In (8), $\sigma = \lambda + i\nu$ and λ and ν are the complex growth factor and angular frequency, respectively. The thermocline perturbation $\tilde{h}$ and the zonal velocity perturbation $\tilde{u}$ are determined from the time-dependent shallow water equations with nonzero damping and forced by the perturbation wind stress

$$\tilde{\tau}^x = \mu\tilde{A}(\tilde{T})e^{-(1/2)\alpha y^2}, \quad (9)$$

in which the meridional extension of the perturbations is taken into account for nonzero α. By the use of Green's functions, similar to those used in Neelin and Jin (1993), both $\tilde{h}$ and $\tilde{u}$ can be expressed through integral operators into $\tilde{T}$. For $\delta = 0$ (the fast wave limit), $\alpha = 0$, $r = 0$, and $a_u = 0$ the Jacobian matrix associated with the steady equations (6) is equivalent with the right-hand side of (7). Changing each of these conditions broadens the class of perturbations that are considered about the particular steady state. The problem of finding branches of steady states and simultaneously one of the eigenmodes $\tilde{T}$ is implemented numerically as follows. The equations for the steady state (5) as well as the real and imaginary parts of the eigenvalue problem (7) are both enforced on an equidistant grid of $M + 1$ points giving $3(M + 1)$ equations. Together with two equations, normalizing the real and imaginary part of the eigenmode, the resulting algebraic equations are written as a bifurcation problem for the $[3(M + 1) + 2]$ vector of unknowns $\mathbf{x}$ defined as

$$\mathbf{x} = (\overline{T}_0, \ldots, \overline{T}_M, \tilde{T}_0^R, \ldots, \tilde{T}_M^R, \tilde{T}_0^I, \ldots, \tilde{T}_M^I, \lambda, \nu). \quad (10)$$

This system of equations is solved by using standard path-following software, in this case the AUTO code (Doedel 1980). In this setup, it is easy to start from an already computed steady state in Part II and determine the eigenmode by homotopy parameters to get a starting point $\mathbf{x}_0$ for the full vector $\mathbf{x}$. Once this is known, both steady state and eigenmode can be followed through parameter space. In all computations below, we take $M = 20$, which gives sufficient accuracy in both the steady states and eigenmodes.

TABLE 1. Standard values of dimensionless parameters.

ϵ_a	2.36	ϵ_T	0.694
α	0.05	T_{so}	24.0
η_1	4.0	T_N	30.0
η_2	0.5	T_O	30.0
r	0.1	δ_s	0.20
α_s	4.0	τ_z	−0.125
δ	1.0	δ_F	4.104

3. Results

a. The ENSO mode and the warm pool–cold tongue climatology

In this section, our aim is to demonstrate that it is possible within this model to obtain ENSO-like unstable modes within a climatology that has a reasonable warm pool–cold tongue structure. This result was obtained for different values of the parameters as those in DN and these values are therefore shown in Table 1. As can be seen from these values, it required some level of tuning, mainly to get the period of the linear oscillation in the correct regime.

In Fig. 1, the real part λ and the imaginary part ν of the growth factor of the most unstable mode, giving growth rate and frequency, respectively, are shown as a function of the coupling strength μ for $\tau_z = -0.125$. Note that time is scaled by L/c_0 and with $c_0 = 2.0$ m s^{-1} and $L = 1.5\ 10^7$ m its value is about 0.24 yr. Hence, the period p^* of a particular mode with frequency ν is calculated from $p^* = 0.48\pi/\nu$ yr. Dimensional growth rates λ^* are calculated from λ through $\lambda^* = \lambda/0.24$ yr^{-1}. In Fig. 1, the mode becomes unstable near $\mu = 1$, while its frequency decreases with increasing μ. Near $\mu = 1$, the steady-state fields $\tilde{A}$, $\tilde{T}$, and $\tilde{h}$ (along the equator) are plotted in Fig. 2. Although the spatial structure of the cold tongue–warm pool configuration is reasonable, the cold tongue is a bit too warm due to the relatively small coupling strength.

Unauthenticated | Downloaded 07/18/24 11:00 AM UTC

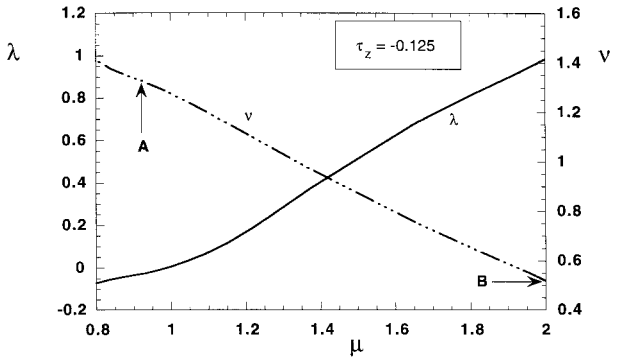

FIG. 1. The dimensionless growth rate λ (solid curve) and the frequency ν (dash–dotted) as a function of coupling strength μ for the leading eigenmode. Standard values of the parameters are as in Table 1. Time is scaled by L/c_0 and with $c_0 = 2.0$ m s^{-1} and $L = 1.5\ 10^7$ m this factor is about 0.24 yr. Hence, the period p^* of a particular mode with frequency ν is calculated from $p^* = 0.48\pi/\nu$ yr. Dimensional growth rates λ^* are calculated from λ through $\lambda^* = \lambda/0.24$ yr^{-1}.

Time–longitude diagrams of the least stable mode at this point (Fig. 3) show that this mode has the features of an ocean basin mode, its period is about 1.1 yr, with slight westward propagation of SST anomalies. In these and the following figures, two periods of the mode are plotted. The time t along the axis is related through the dimensional time t^* through $t = t^*/(2p^*)$. As coupling increases, the cold tongue becomes stronger and the oscillatory mode becomes unstable (Fig. 1). At $\mu = 2$, the cold tongue obtained (Fig. 4) has about the right amplitude with respect to that observed, although the transition occurs a bit too rapidly between warm SST in the west and cold SST in the central and eastern Pacific. The unstable mode (Fig. 5) has a spatial structure that resembles an ENSO mode, for example, as shown in Neelin et al. (1994). The SST anomaly is nearly stationary and has its largest amplitude in the cold tongue region. The thermocline anomaly is nearly stationary with slight eastward propagation near the center of the basin associated with the western Pacific tending to lead the eastern Pacific slightly.

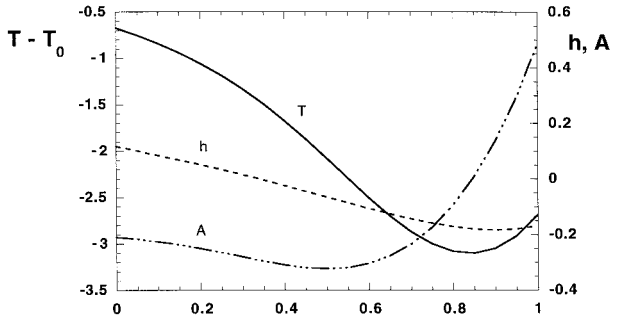

FIG. 2. Spatial structure along the equator of the mean state of the SST $\overline{T}$, the wind stress $\overline{A}$, and the thermocline $\overline{h}$ at the point labeled A ($\mu = 0.90$) in Fig. 1. SST is in K, shown relative to the surface flux equilibrium value T_0. Here $\overline{A}$ and $\overline{h}$ are nondimensional and are relative to the external wind stress and resting ocean state, respectively.

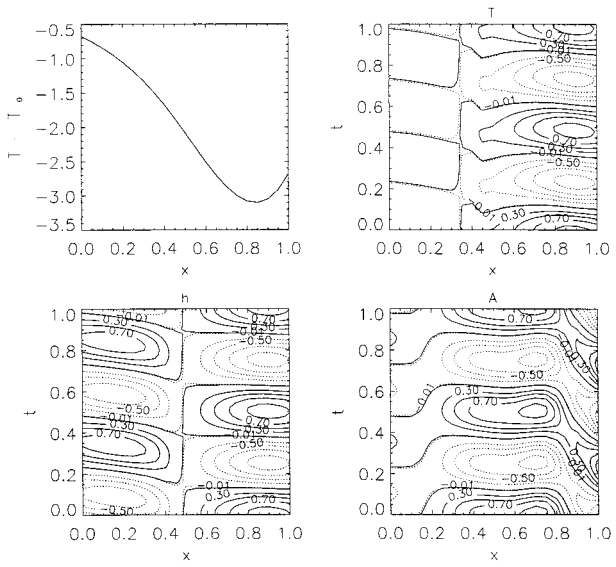

FIG. 3. Structure along the equator of the mean state of the SST (top left) $\overline{T} - T_0$ in *K*. (top right) Time–longitude diagrams along the equator of the most unstable mode perturbation for SST, (bottom left) thermocline depth, and (bottom left) the wind stress anomalies at the point labeled A in Fig. 1. The period p^* of the mode is 1.1 yr. In these and the similar figures below, two periods of the mode are plotted. The time t along the axis is related through the dimensional time t^* through $t = t^*/(2p^*)$. The contour plots have been scaled with the maximum values of the field, and contour values are with respect to this value.

The period of oscillation for the mode in Fig. 5 is about 3.5 yr but, as can be seen in Fig. 1, this period changes significantly with coupling strength. In addition, it is sensitive to other parameters in the system, as is the spatial structure of the climatology. If either δ_s or ϵ_a is changed too much, the climatology becomes unrealistic. In short, the simultaneous occurrence of desirable characteristics of the ENSO mode in Fig. 5, with the right period, and a coupled climatology that has an adequate cold tongue structure is not found over a large volume in parameter space. Starting from the earlier

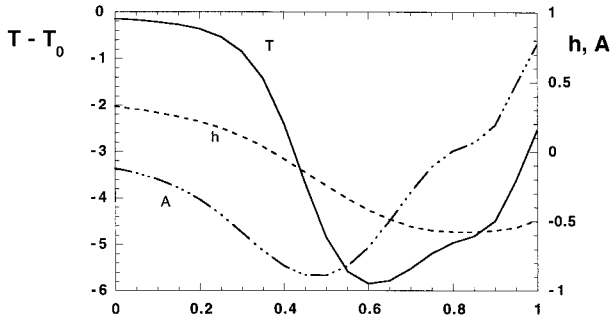

FIG. 4. Spatial structure along the equator of the mean state of SST, $\overline{T}$, wind stress $\overline{A}$, and thermocline $\overline{h}$ at the point labeled B ($\mu = 2.06$) in Fig. 1. Format as in Fig. 2.

Unauthenticated | Downloaded 07/18/24 11:00 AM UTC

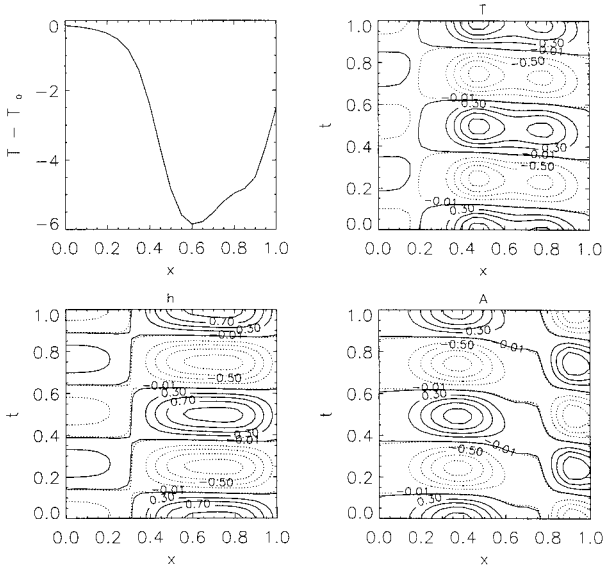

FIG. 5. As in Fig. 3 but for mean state of SST, $\overline{T} - T_0$; most unstable mode SST anomaly, thermocline depth anomaly; and wind stress anomaly at the point labeled B in Fig. 1. The period of the mode is 3.5 yr.

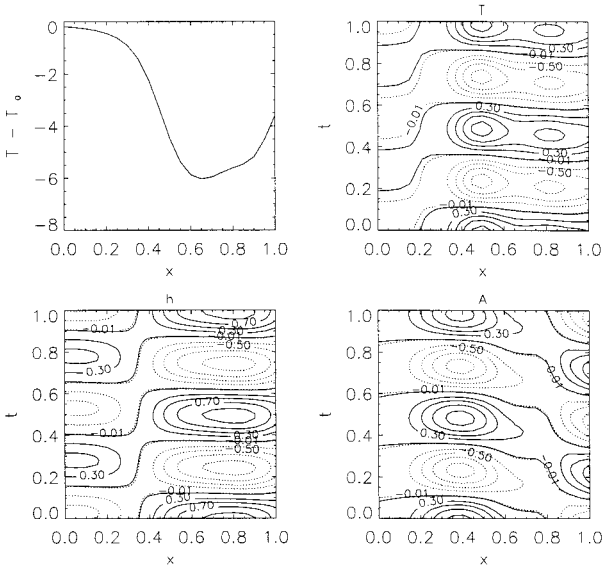

FIG. 7. As in Fig. 3 but for mean state of SST, $\overline{T} - T_0$; most unstable mode SST anomaly, thermocline depth anomaly; and wind stress anomaly at the point labeled A ($\mu = 1.74$) in Fig. 6. The period of the mode is 1.6 yr.

results in ND, a number of simultaneous adjustments were necessary to obtain this state.

b. *Externally imposed versus internally generated wind stress*

One of the important hypotheses underlying the coupled model is that wind stress due to factors outside the basin, the external wind stress, generates a zonal SST gradient in the absence of coupling, which is then magnified and modified by the coupled feedbacks. The sensitivity of the climatology to the magnitude of this external wind stress component was studied in DN, where it was shown that having sufficient magnitude of τ_z had an important impact on whether a correct cold tongue could be generated. The standard case discussed above is for $\tau_z = -0.125$. In Fig. 6, the leading mode is plotted for the case $\tau_z = -0.15$ and although the mode still becomes unstable at sufficiently large coupling, the frequency remains quite large. The patterns of the climatological SST and the time–longitude diagrams of the most unstable mode for $\mu = 1.7$ (Fig. 7) seem qualitatively correct, but the period of the oscillation never increases above 1 yr.

When τ_z is changed to -0.1, it is found (Fig. 8) that the frequency decreases to zero and the oscillatory mode bifurcates into two stationary modes. In this case, the stationary modes merge again at larger μ to give another oscillatory mode. As noted in DN, nonoscillatory modes can pass through zero eigenvalue only under very particular circumstances (which almost never happen) when the climatology is also coupled. However, nothing disallows growing stationary modes if they arise from an oscillatory mode that has already gone unstable, as

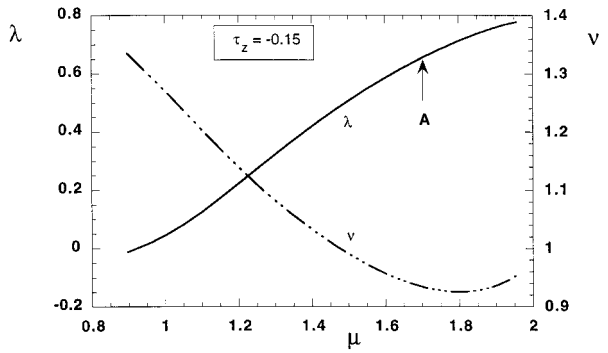

FIG. 6. As Fig. 1 but for a different value of the external wind stress $\tau_z = -0.15$.

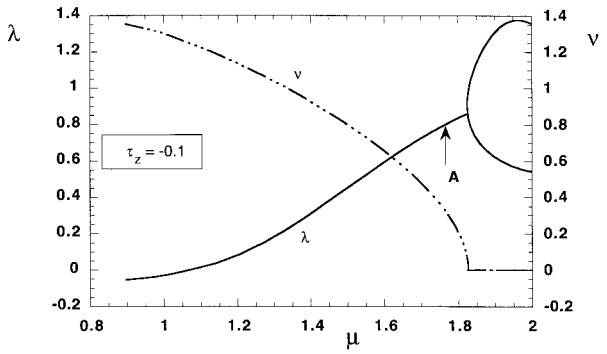

FIG. 8. As in Fig. 1 but for a different value of the external wind stress $\tau_z = -0.1$.

Unauthenticated | Downloaded 07/18/24 11:00 AM UTC

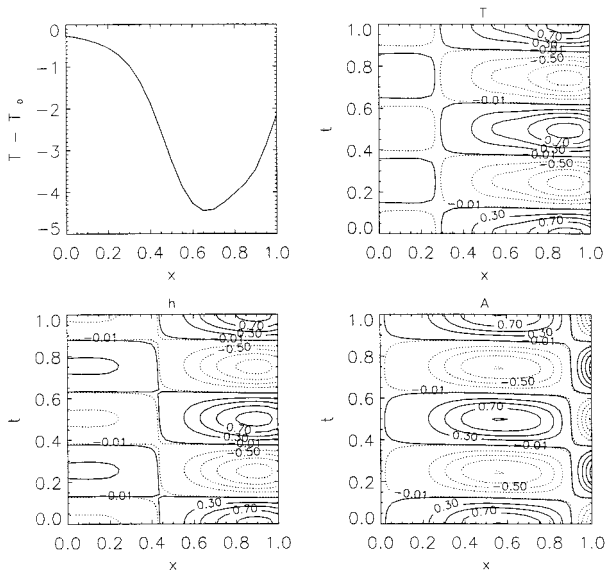

FIG. 9. As in Fig. 3 but for mean state of SST, $\overline{T} - T_0$; most unstable mode SST anomaly, thermocline depth anomaly; and wind stress anomaly at the point labeled A ($\mu = 1.81$) in Fig. 8. The period of the mode is 10.1 yr.

in Fig. 8. The splitting of the oscillatory, ENSO-like mode into growing stationary modes as coupling increases in Fig. 8 is very much like the situations found in JN. Essentially, for strong coupling, local growth processes occur so fast that effects of wave dynamics are no longer sufficient to give oscillation. The pattern at $\mu = 1.8$ in Fig. 8, shown in Fig. 9, has a nice SST climatology and indicates that the oscillatory mode has a nearly stationary oscillation in SST. The temperature difference between warm pool and cold tongue is smaller in Fig. 9 than in Fig. 7 or Fig. 5. This is expected since the feedbacks within the basin do depend on the size of the ''seed'' provided by τ_z, and this is smaller in the case of Fig. 9. Climatological upwelling is thus less intense in Fig. 9, so why do the feedbacks in the ENSO mode appear stronger? The answer lies in the climatological thermocline depth and how shallow it becomes in the east. The T_s parameterization (shown in Fig. 12) saturates if the thermocline becomes very shallow, since upwelled temperatures cannot get much colder. This results in dT_s/dh becoming small in the east, so that small thermocline perturbations do not change the SST tendency as strongly. There is thus a trade-off affecting the ENSO mode as coupling becomes stronger. The direct effect of larger coupling on the modes tends to create a stronger feedback via winds and thermocline dynamics upon SST. However, if the effect of larger coupling on the climatology is to shoal the thermocline strongly in the east, it actually reduces the thermocline feedback effects for perturbations.

As parameters are changed they affect the coupled mode directly, as in the flux-corrected problem, but they also affect the mode via the changes in climatology. The climatological upwelling rate $\overline{w}$, $\overline{T}_{\text{sub}}$ and the climatological SST pattern determine the extent of the SST anomaly, and experience from the flux-corrected problem suggests that $\overline{w}$ and $\overline{T}_{\text{sub}}$ strongly affect the period. However, a comparison of the patterns in both Figs. 5 and 7 indicates that the interplay of parameters and climatology in determining properties of the mode can be subtle. The mode in Fig. 7 has a consistently smaller period than the mode in Fig. 5 even though the spatial characteristics do not appear very different. The reason is that the spatial form is dominated by near-stationary balances, and the signature on the equator of the memory of the mode is relatively small. The mode in Fig. 5 has more of an SST mode character and thus larger period, but both are mixed SST–ocean dynamics modes. Some paths characterizing this mixing are discussed below.

1) CONNECTION BETWEEN THE SST AND OCEAN DYNAMICS MODES

As is known from stability analyses of flux-corrected climatologies in JN, ENSO-like unstable modes have mixed properties of stationary SST modes—which could be studied in the fast wave limit—and oscillatory modes resulting from the spectrum of the shallow water equations. In the coupled case, the latter set of modes consists of two subsets: discrete modes of the equations in the long-wave approximation in the ocean basin modes and a set of modes that arises from a discretized continuous spectrum, called the ''scattering spectrum.'' Simple cases of merging of the two different type of modes were found to be related to the connection of the eigensurfaces of a stationary SST mode and a particular scattering mode at low δ and with a particular ocean basin mode at larger δ. In the model used here, the scattering modes are essentially filtered at low coupling through the exact summation of the Green's function. Hence, when we consider the low coupling limit in this model, connections of the mixed SST–ocean dynamics mode to the ocean dynamics spectrum will appear to be always to the ocean basin mode, rather than to the continuum spectrum. From the results of JN, we know there is a region at small coupling where both subsets of the ocean dynamics spectrum become rapidly mixed. Thus we interpret the low coupling connections to the ocean basin modes as connections to the ocean dynamics spectrum in general.

To demonstrate in a simple way that the unstable mode in Fig. 1 originates from mixed properties of SST modes and ocean dynamics modes, we follow the eigenvalue curves as a function of the parameter δ that does not affect the climatology. For example, in the case $\tau_z = -0.1$ and $\alpha = 0$, three slices for different δ (Fig. 10) show the connection between both classes of modes. It turns out that some of these branches are difficult to compute numerically over the whole μ interval due to the occurrence of two degeneracies (here a bifurcation

Unauthenticated | Downloaded 07/18/24 11:00 AM UTC

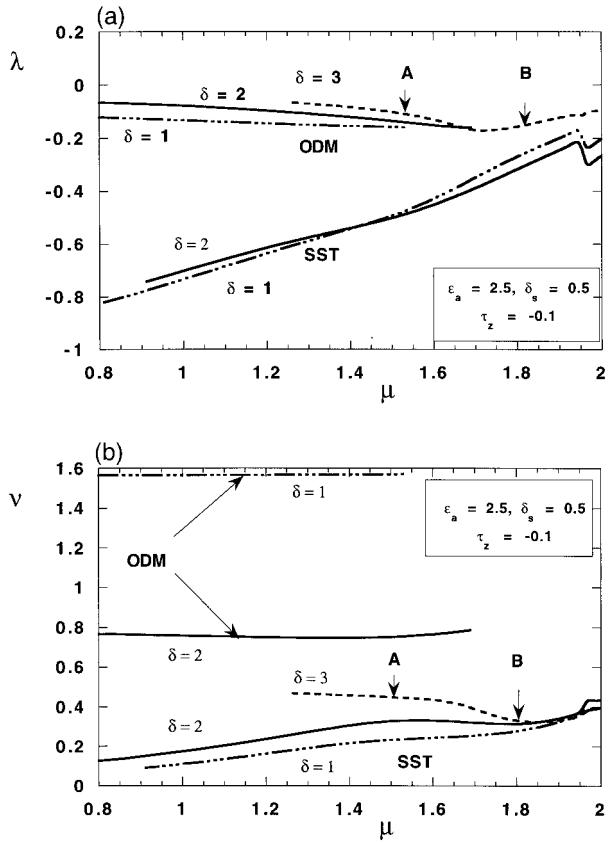

FIG. 10. (a) Growth factor and (b) frequency as a function of coupling strength for three values of δ. In both panels, ODM and SST indicate ocean dynamics and SST modes, respectively.

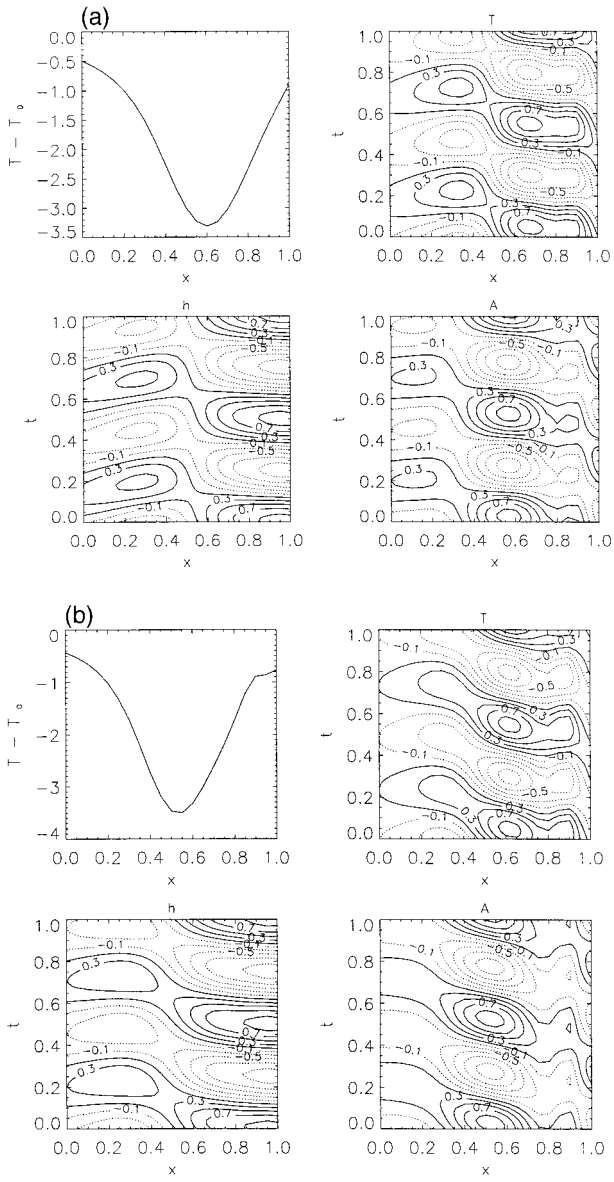

FIG. 11. (top left) Structure along the equator of the mean SST, $\overline{T} - T_0$ and (top right) time–longitude diagrams for the eigenmode SST perturbation, (bottom left) thermocline perturbation, and (bottom right) wind stress perturbation. In (a), the mode at the points labeled A ($\mu = 1.54$) in Fig. 10 is shown and in (b), the mode at the points labeled B ($\mu = 1.78$) in Fig. 10 is shown.

of two oscillatory branches). With increasing δ, the ocean dynamics mode approaches the SST mode and for $\delta = 3$ both branches have connected. For this value of δ, the spatiotemporal patterns of the most unstable mode are plotted for two values of μ (Fig. 11) to show the smooth transition of the patterns of both classes of modes. At $\mu = 1.5$, the climatology (Fig. 11a) has a cold tongue that is shifted too much to the west. Consequently, the temperature signal of the mode, which still has a pattern corresponding to the ocean dynamics mode, is also shifted to the west. For $\mu = 1.8$ (Fig. 11b) westward-propagating tendencies associated with the SST mode can be noticed, showing the mixing of properties between the two classes of modes. For even larger μ, eastern warming occurs and the modes begin to have an unrealistic spatial pattern.

2) THE IMPACT OF THE SUBSURFACE TEMPERATURE PARAMETERIZATION

Both the climatology and the character of the modes can be very sensitive to the shape of the T_s function in Eq. (2). Several shapes have been used in the past, and in addition to that taken from Neelin and Jin (1993) as a standard case in ND, in this paper the one used by Jin (1996) was considered (Table 1). For this parameterization, the values of the offset, steepness as well as the bounding temperatures are slightly changed. Both functions T_s are displayed in Fig. 12, where the one in ND will be indicated by T_s^o (solid curve in Fig. 12) and the one by Jin (1996) by T_s^n (dash–dotted curve in Fig. 12). The main difference between both curves is that saturation at the cold end is at higher temperatures and the gradient is smaller.

Using the shape of T_s^o, it turns out that the optimum climatology of DN is completely stable and that the

Unauthenticated | Downloaded 07/18/24 11:00 AM UTC

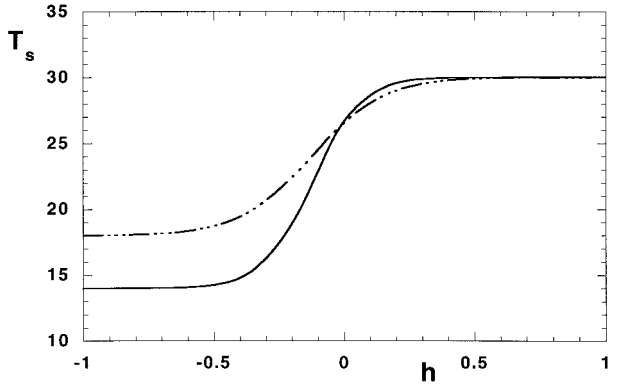

FIG. 12. The distribution of the subsurface temperature T_s as a function of thermocline depth h, as used in this paper, T_s^n, (dash–dotted curve) and that used in DN, T_s^o, (solid curve).

eigensurfaces associated with the ocean basin mode and SST modes are for the most part unconnected. Figure 13a shows the bifurcation diagram for the climatology for both of the T_s functions in Fig. 12. On the y axis, the deviation of the temperature in the cold tongue with respect to the externally induced temperature (by τ_{ext}) is plotted, that is, $T_{\text{EC}} = \overline{T}_{\text{EC}} - \overline{T}_{\text{EC}}^{\text{ext}}$ similar to Fig. 3 in ND. In both cases, the cold tongue temperature becomes colder as coupling increases by the mechanisms discussed in DN. At the same value of μ, the new parameterization produces a warmer cold tongue because the temperature of the subsurface water is warmer (Fig. 12). Hence for T_s^n, thermocline deviations sufficiently strong such that the cold tongue is as cold as observed occur at larger μ.

For the eigenmodes, we consider the simplest case with $a_u = 0$, $r = 0$, $\alpha = 0$, $\delta = 1$ and also neglect the effect of the mean vertical velocity perturbation in the SST equation. In this case, the growth factor λ and angular frequency ν are plotted in Figs. 13b and Fig. 13c, respectively. Note that for $\mu \downarrow 0$, all SST modes approach $\lambda \downarrow -(\epsilon_T - \delta_F \tau_z)$ and $\nu = 0$, whereas the ocean dynamics mode approaches $\lambda = 0$, $\nu = \pi/2$. The SST climatology and the time–longitude plot of the SST perturbation corresponding to the ocean dynamics mode at $\mu = 0.7$ is shown in Fig. 14a. The climatological SST distribution shows a pronounced cold tongue–warm pool structure (Fig. 14a) of which the physics was discussed at length in DN. For large μ, the growth rate of this mode becomes very small negative (i.e., weak decay), but it does not become positive. The SST modes are all stable and stationary up to $\mu \simeq 0.7$. At larger μ, two stationary modes merge to generate a westward-propagating oscillatory mode, but this mode is not the most unstable SST mode until $\mu > 0.95$. For larger μ, the upwelling feedback introduces an eastern warming shifting the cold tongue to the west and the SST pattern becomes very unrealistic (shown for $\mu = 1.0$ in Fig. 14b).

Thus with the T_s^o parameterization we found no regions with unstable, realistic ENSO modes and realistic

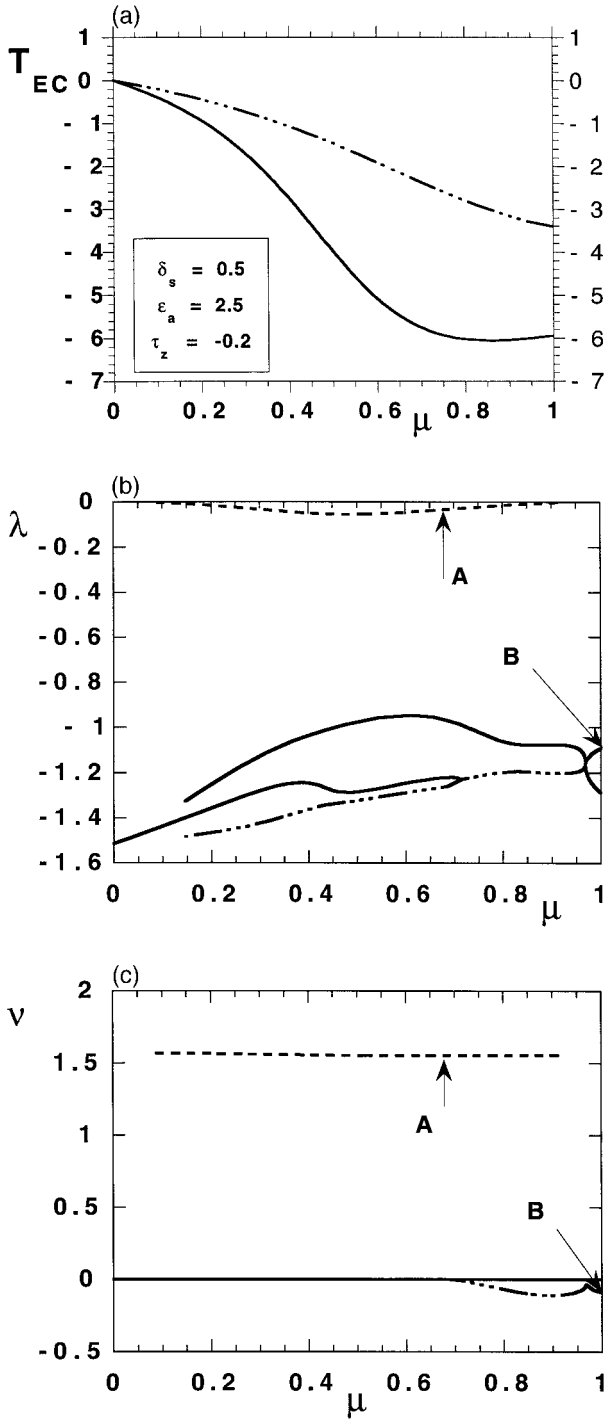

FIG. 13. (a) Value of the climatological SST at $x = 0.7$ with respect to the externally induced temperature ($T_{\text{EC}} = \overline{T}_{\text{EC}} - \overline{T}_{\text{EC}}^{\text{ext}}$) as a function of coupling strength for the optimal values of the parameters as in DN and two different shapes of T_s as in Fig. 12. (b) Growth rate of the most unstable modes as a function of μ. (c) Frequency of the most unstable modes as a function of μ. Fewer curves are seen in (c) because more than one mode has zero frequency.

Unauthenticated | Downloaded 07/18/24 11:00 AM UTC

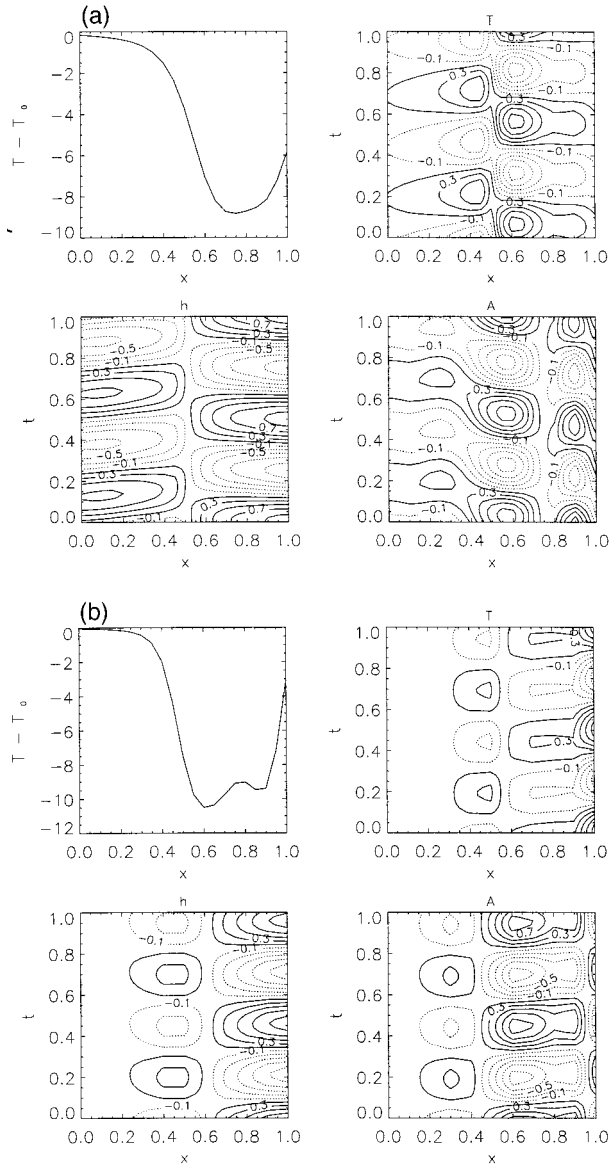

FIG. 14. (top left) Structure along the equator of the mean SST, $\overline{T} - T_0$, and (top right) time–longitude diagrams for the eigenmode SST perturbation, (lower left) thermocline perturbation, and (lower right) wind stress perturbation. (a) The mode at the points labeled A ($\mu = 0.68$, period 1 yr) in Figs. 13b,c is shown, and (b) the mode at the points labeled B ($\mu = 1.0$, period 10 yr) in Figs. 13b,c is shown.

climatology. The modest change in T_s parameterization of Fig. 12 makes an enormous difference in this respect. As discussed at the beginning of this section, this is due to the tendency to nonlinear saturation of the T_{sub} parameterization for shallow thermocline depths in the eastern basin. In the climatology of Fig. 4, the values of h in the east may be seen to lie on the part of the old parameterization (solid curve) in Fig. 12 that is almost saturated, while the new parameterization (dash–dotted curve) still has an appreciable dT_s/dh. While the new parameterization is more realistic, deficiencies in the old parameterization were less apparent when used either to study variability alone in the flux-corrected case or to study the coupled climatology alone without considering variability.

One caveat should, however, be noted in discussing this sensitivity. Linear periods tend to be more sensitive than nonlinear periods in these models. If El Niño can be maintained by weather noise (Eckert and Latif 1997; Blanke et al. 1997), finite-amplitude noise-induced perturbations would be able to depress the thermocline sufficiently to cause T_s variations even for very shallow climatological thermocline. Thus the El Niño in a full model might be less sensitive than indicated by these linear mode studies. However, the qualitative point remains that obtaining both climatology and interannual variability simultaneously is a significantly more demanding problem than simulating only one.

4. Discussion and conclusions

The spatial pattern of the annual-mean state is central to the shape and frequency of its oscillatory instabilities and both depend strongly on coupled ocean–atmosphere feedbacks. In this third part of a series of papers, the relationship between these two features of the tropical climate system are investigated. We use an intermediate coupled ocean–atmosphere model—a stripped-down version of the Zebiak–Cane model—to examine the linear stability of fully coupled, nonlinear climatologies. An approximation is used that filters out the scattering spectrum of the uncoupled ocean, which may oversimplify the analysis of instabilities at low coupling, but we believe we understand these effects from previous analysis in the flux-corrected case (Jin and Neelin 1993a; Neelin and Jin 1993). Using techniques of bifurcation theory, we are able to follow both mean state and one of the eigenvalue branches simultaneously in parameter space.

At small coupling, the structure of the mean state is to a large extent determined by the zonally constant external wind stress τ_{ext}. This mean state is stable to both SST modes, which might be oscillatory or stationary (i.e., nonoscillatory), and oscillatory ocean basin modes. The latter are the only ocean modes in the filtered ocean model from the shallow water spectrum on the equatorial β plane. As coupling increases, the coupled feedbacks within the Pacific basin modify this externally imposed mean state to a fully developed cold tongue–warm pool structure. The externally induced zonal SST gradient causes an increase of the easterlies, which in turn cause the thermocline to steepen. In the presence of sufficient upwelling, the thermocline anomalies affect the SST field. Surface layer processes may modify the actual shape of the SST modification relative to that externally induced by affecting the upwelling structure directly. These processes are similar to those described in more detail in DN.

Unauthenticated | Downloaded 07/18/24 11:00 AM UTC

Simultaneously, with increasing coupling, the structures of the uncoupled ocean basin modes and SST modes are substantially modified and take on properties of mixed SST–ocean dynamics modes. These modes tend to be destabilized by coupling and in some parameter regions, the leading mode becomes unstable. Systematic searches of the reasonable parameter range led to a parameter regime where both the spatial structure of the mean state has the correct east–west contrast and the unstable mode has ENSO-like characteristics. This mode has mixed SST–ocean dynamics mode properties. The ''mixed mode'' terminology was suggested by JN because in the flux-corrected case, eigensurfaces of the realistic ENSO mode are connected both to the ocean dynamics spectrum and the SST modes. A similar connection of the eigensurfaces of both the ocean basin mode and SST modes was demonstrated here by varying parameters not affecting the climatology, for example, the ratio (δ) of ocean adjustment processes versus adjustment of SST. At small δ, SST modes and ocean dynamics modes do not join as coupling is increased. For larger δ, modes that begin at zero coupling as an ocean basin mode and an SST mode, respectively, merge as coupling increases. Mergers with the ocean scattering spectrum noted in JN are filtered out here by the approximation used, but presumably would occur similarly.

The connections of eigensurfaces are thus qualitatively similar in many respects to the flux-corrected case of JN. However, a significant difference in this coupled climatology case is that stationary (nonoscillatory) modes cannot have zero eigenvalue, that is, cannot go from stable to unstable, because transcritical bifurcations from the mean state no longer occur in the coupled case as they do in the flux-corrected case (ND). We have noted some cases where the climatology develops a limit point (as a coupling strength is varied), which allows neutral stationary modes, but this occurs for very unrealistic climatologies and is therefore considered to be irrelevant. Unstable stationary modes can occur but it is always oscillatory modes that cross the stability boundary.

We find that the period of the oscillation has a complicated dependence on parameters because the climatology changes simultaneously, as do the balances between coupled feedbacks that generate this climatology. We show an example (Figs. 5 and 7) where the climatologies do not differ very much and the shape of the unstable modes also corresponds well, and yet in one case the mode has a significantly larger period. This difference is caused by a slight increase of the amplitude of the external wind stress τ_{ext}. Coupled feedbacks within the climatology amplify this external increase in upwelling and thermocline tilt. Although the climatology changes are very modest, further nonlinear saturation of the thermocline feedback in the modified climatology tends to decrease the effect of this feedback for perturbations. This modifies the character of the unstable mode. In DN, we have provided scenarios for how errors in climatologies in coupled GCMs can be understood as exacerbations of errors in parameters or in the uncoupled components. The results here provide an example of how a change or error in the mean state can impact the variability in the coupled system, via feedbacks that make the original error difficult to trace.

In summary, we underline these main points.

1) It is possible to obtain a reasonable simulation of the warm pool–cold tongue climatology simultaneously with an unstable interannual ENSO mode. The climatology depends significantly on coupled feedbacks akin to those at work in the ENSO mode, as found in DN.

2) The ENSO mode is a mixed SST–ocean dynamics mode that arises by connections of modes in parameter space similar to those found in the flux-corrected case in JN. The ENSO mode combines properties from the ocean dynamics spectrum and strongly coupled SST modes. The main modification is that when the climatology is coupled, only oscillatory modes can cross the boundary from stability to instability. Stationary (i.e., nonoscillatory) modes cannot (normally) because the coupled feedbacks modify the climatology rather than produce a bifurcating stationary solution.

3) However, at least in this model, there is only a restricted range of parameters where one simultaneously finds a coupled climatology similar to observed, an ENSO mode of observed spatial form and period, and instability of the ENSO mode. In the flux-corrected problem, a slight inaccuracy in a parameterization does not strongly affect the shape of the climatological cold tongue and thermocline tilt, and these in turn strongly constrain the spatial form of the ENSO mode. In the fully coupled problem, inaccuracies in a parameterization affect the spatial shape of the coupled climatology, and this can adversely affect simulation of the ENSO mode. However, even when the parameterizations provide a balance of mechanisms that give a reasonable climatology, this does not necessarily lead to an unstable ENSO mode of correct period. For instance, in this model, as in ZC and JN, the dependence of upwelled subsurface temperature on thermocline depth has a nonlinear saturation when thermocline depth becomes very shallow, since upwelled water can become no colder. If this saturation effect occurs too sharply in the parameterization, then when the climatology is reasonably simulated, the thermocline feedback in the eastern basin is too weak to produce a low-frequency, unstable ENSO mode. In a flux-corrected model, increased coupling could be used to compensate for this in the ENSO mode, but in the fully coupled case this adversely impacts climatology. This strong impact of an apparently small change in the subsurface temperature parameterization illustrates that tuning model parameters to improve aspects of the climatology does not necessarily simultaneously improve the variability. This may be relevant to coupled GCM simulations, where it is commonly found that a reasonable simulation of climatology is not

Unauthenticated | Downloaded 07/18/24 11:00 AM UTC

necessarily associated with a good ENSO simulation, and vice versa (Mechoso et al. 1995). The results here suggest that the fully coupled problem is much more demanding than the flux-corrected problem in terms of the required accuracy of model parameterizations. They also suggest that some of the interdecadal longer-term variability of ENSO period and amplitude may be due to relatively small external influences being amplified in the Pacific coupled climatology by feedbacks similar to those at work in ENSO itself.

Acknowledgments. The work of HD was supported by the Dutch National Research Programme on Global Air Pollution and Climate Change (N.R.P.) within Project 951235. All computations were performed on the CRAY C90 at the Academic Computing Centre (SARA), Amsterdam, the Netherlands, within Project SC283. Use of these computing facilities was sponsored by the National Computing Facilities Foundation (N.C.F.) with financial support from the Netherlands Organization for Scientific Research (N.W.O). This work was initiated and completed during visits of HD to UCLA in 1993, 1996, and 1997 and sponsored by NSF Grant ATM-9521389 and a N.W.O. PIONIER grant. Discussions with Fei-Fei Jin are much appreciated.

APPENDIX A

Coefficients in Eq. (7)

The basic-state vertical velocity $\overline{w}_1$ and the meridional velocity $\overline{v}_N$ can be written as

$$\overline{w}_1 = -[\delta_F \tau_{\text{ext}} + \mu\delta_s A(\overline{T} - T_0)],$$
$$\overline{v}_N = -\overline{w}_1. \tag{A1}$$

Let $f(x) = \frac{1}{2}[1 + \tanh(x/\epsilon)]$ be the approximation of the Heaviside function for small ϵ. Then the coefficients $a_T(x)$, $a_h(x)$, $a_w(x)$, $a_v(x)$, and $a_u(x)$ in Eq. (7) are given by

$$a_T = \epsilon_T + \overline{v}_N f(\overline{v}_N) + \overline{w}_1 f(\overline{w}_1),$$
$$a_w = (f(\overline{w}_1) + \overline{w}_1 f'(\overline{w}_1))[\overline{T} - T_s(\overline{h})],$$
$$a_v = f(\overline{v}_N) + \overline{v}_N f'(\overline{v}_N)(\overline{T} - T_N),$$
$$a_u = \frac{\partial \overline{T}}{\partial x},$$
$$a_h = \overline{w}_1 f(\overline{w}_1)\frac{\partial \overline{T}_s}{\partial h}(\overline{h}). \tag{A2}$$

In (7), the perturbation quantities for the vertical and meridional velocity are expressed as

$$\hat{w}_1 = -\mu\delta_s A(\hat{T}) + \alpha_s \hat{w},$$
$$\hat{v}_N = -\hat{w}_1, \tag{A3}$$

with $\alpha_s = H/H_1$. The expressions for $\hat{u}$, $\hat{h}$, and $\hat{w}$ in terms of $\hat{T}$ are obtained using the appropriate Green's functions (Neelin and Jin 1993).

APPENDIX B

Green's Function Correction in Case $\alpha \ll 1$

The problem at hand is to find a closed form expression for solutions to the equations

$$\delta\sigma u + ru + yv + h_x = \tau(x)e^{-(\alpha/2)y^2},$$
$$yu + h_y = 0,$$
$$\delta\sigma h + rh + u_x + v_y = 0, \tag{B1}$$

with the boundary conditions

$$u(1, y) = 0, \qquad \int_{-\infty}^{\infty} u(0, y)\, dy = 0,$$

and all quantities bounded as $y \to \pm\infty$. For $\alpha = 0$, a closed form solution was given in Neelin and Jin (1993). It seems that no closed form solution can be given for general α; hence we turn to an asymptotic correction in case $\alpha \ll 1$. The procedure followed is similar to that in Neelin and Jin (1993) and only details involving the correction are given.

For general α, the solution to the problem (B1) is given by

$$\mathbf{u}(x, y, t) = \int_0^1 \mathbf{G}(x, y; x_0)\tau(x_0)\, dx_0, \tag{B2a}$$

with $\mathbf{u} = (u, h)$ and $\mathbf{G} = (G_u, G_h)$ the Green's function associated with the problem (B1). This vector function is given by

$$\mathbf{G}(x, y; x_0) = b_N \mathbf{K}_N(\phi(x - 1), y) + \mathcal{H}(x_0 - x) \times \left[\sum_{n=0}^{N} (2n + 1) r_n \mathbf{R}_n e^{i\phi(x-x_0)(2n+1)} - d_K \mathbf{M}_K e^{-i\phi(x-x_0)}\right]. \tag{B2b}$$

In this equation $\phi = -i(\delta\sigma + r)$, the $\mathbf{M}_K$ and $\mathbf{R}_n$ are the normalized Kelvin and Rossby vector functions given, for example, in appendix B of Neelin and Jin (1993) and the vector function $\mathbf{K}_N$ is defined as

$$\mathbf{K}_N(p, y) = \mathbf{M}_K e^{-ip} + \sum_{n=0}^{(N-1)/2} 2\gamma_{2n+1}\mathbf{R}_{2n+1}e^{ip(4n+3)}. \tag{B2c}$$

The coefficients d_K, r_n, and γ_{2n+1} are given by

$$d_K = \frac{\pi^{1/4}}{[(1 + \alpha)]^{1/2}}; \qquad \gamma_{2n+1} = (2^n n!)^{-1}[(2n + 1)!]^{1/2}$$

$$r_{2n+1} = -2\gamma_{2n+1}\frac{\pi^{1/4}}{[(1 + \alpha)]^{1/2}}\frac{(1 - \alpha)^n}{(1 + \alpha)^{n+1}}\left(\alpha + \frac{1}{4n + 3}\right);$$
$$r_{2n} = 0. \tag{B2d}$$

Unauthenticated | Downloaded 07/18/24 11:00 AM UTC

Finally, the coefficient b_N in (B2b) is determined by the zero mass flux condition on the western boundary and the limit $N \to \infty$ is taken.

To obtain a correction in α, first the coefficients in (B2d) are expanded in α to get

$$d_K = \pi^{1/4}\left[1 - \frac{\alpha}{2} + O(\alpha^2)\right];$$

$$r_{2n+1} = -2\gamma_{2n+1}\pi^{1/4}\left[\frac{1}{4n+3} + \frac{\alpha}{2} + O(\alpha^2)\right]. \quad \text{(B3)}$$

When the expansions for d_K and r_{2n+1} are substituted into the Green's function expression, one obtains

$$\mathbf{G}(x, y; x_0) = b_N\mathbf{K}_N(\phi(x-1), y) - \pi^{1/4}\mathcal{H}(x_0 - x) \times \left\{\mathbf{K}_N[\phi(x-x_0), y] - i\frac{\alpha}{2}\frac{\partial \mathbf{K}_N}{\partial p}[\phi(x-x_0), y]\right\}, \quad \text{(B4)}$$

where $\partial\mathbf{K}_N/\partial_p$ denotes differentiation with respect to the first argument. To obtain a closed form solution of the right-hand side of (B4) in the limit $N \to \infty$, with $\mathbf{K} = \lim_{N\to\infty}\mathbf{K}_N$, we make use of the identity

$$\mathbf{K}(p, y) = \pi^{-1/4}(\cos 2p)^{-1/2}e^{(y^2/2)i\,\tan 2p}(-i\sin 2p, \cos 2p) = \mathbf{M}_K e^{-ip} + \sum_{n=0}^{\infty} 2\gamma_{2n+1}\mathbf{R}_{2n+1}e^{ip(4n+3)}. \quad \text{(B5a)}$$

When (B5a) is differentiated with respect to the argument p, we obtain another identity

$$i\frac{\partial \mathbf{K}}{\partial p} = \mathbf{M}_K e^{-ip} - \sum_{n=0}^{\infty} 2\gamma_{2n+1}(4n+3)\mathbf{R}_{2n+1}e^{ip(4n+3)} = \pi^{1/4}\frac{e^{(y^2/2)i\,\tan 2p}}{(\cos 2p)^{3/2}} \times (1 + \cos^2 2p + iy^2\tan 2p, -y^2 - i\sin 2p\cos 2p). \quad \text{(B5b)}$$

Hence, up to $O(\alpha)$ a closed form solution can be obtained for the Green's function. The coefficient $b = \lim_{N\to\infty} b_N$ is given by

$$b = \pi^{1/4}\left(\frac{\sin 2\phi x_0}{\sin 2\phi}\right)^{1/2}\left[1 - \frac{\alpha}{2}\left(\frac{2 + \cos^2 2\phi x_0}{\cos 2\phi x_0}\right)\right]. \quad \text{(B6)}$$

Once b is determined, the solutions u and h can be obtained through (B4) and the original equation (B2a).

REFERENCES

Battisti, D., and A. C. Hirst, 1989: Interannual variability in a tropical atmosphere–ocean model: Influence of the basic state, ocean geometry, and nonlinearity. *J. Atmos. Sci.,* **46,** 1687–1712.

Blanke, B., J. D. Neelin, and D. Gutzler, 1997: Estimating the effects of stochastic wind stress forcing on ENSO irregularity. *J. Climate,* **10,** 1473–1486.

——, M. Münnich, and S. Zebiak, 1990: Study of self-excited oscillations of the tropical ocean–atmosphere system. Part I: Linear analysis. *J. Atmos. Sci.,* **47,** 1562–1577.

Cane, M. A., A. C. Clement, A. Kaplan, Y. Kushnir, D. Pozdnyakov, R. Seager, S. E. Zebiak, and R. Murtugudde, 1997: Twentieth-century sea surface temperature trends. *Science,* **275,** 957–960.

Chang, P., B. Wang, T. Li, and L. Ji, 1994: Interactions between the seasonal cycle and the Southern Oscillation—Frequency entrainment and chaos in an intermediate coupled ocean–atmosphere model. *Geophys. Res. Lett.,* **21,** 2817–2820.

——, L. Ji, B. Wang, and T. Li, 1995: Interactions between the seasonal cycle and El Niño–Southern Oscillation in an intermediate coupled ocean–atmosphere model. *J. Atmos. Sci.,* **52,** 2353–2372.

Dijkstra, H. A., and J. D. Neelin, 1995a: On the attractors of an intermediate coupled ocean–atmosphere model. *Dyn. Atmos. Oceans,* **22,** 19–48.

——, and ——, 1995b: Coupled ocean–atmosphere models and the tropical climatology. Part II: Why the cold tongue is in the east. *J. Climate,* **8,** 1343–1359.

Doedel, E., 1980: AUTO: A program for the automatic bifurcation analysis of autonomous systems. *Proc. 10th Manitoba Conf. Numer. Math. Comput.,* **30,** 265–274.

Eckert, C., and M. Latif, 1997: Predictability of a stochastically forced hybrid coupled model of the tropical Pacific ocean–atmosphere system. *J. Climate,* **10,** 1488–1504.

Gill, A., 1980: Some simple solutions for heat induced tropical circulation. *Quart. J. Roy. Meteor. Soc.,* **106,** 447–462.

Hao, Z., J. D. Neelin, and F.-F. Jin, 1993: Nonlinear tropical air–sea interaction in the fast-wave limit. *J. Climate,* **6,** 1523–1544.

Hirst, A. C., 1986: Unstable and damped equatorial modes in simple coupled ocean–atmosphere models. *J. Atmos. Sci.,* **43,** 606–630.

——, 1988: Slow instabilities in tropical ocean basin-global atmosphere models. *J. Atmos. Sci.,* **45,** 830–852.

Jin, F.-F., 1996: Tropical ocean–atmosphere interaction, the Pacific cold tongue, and the El Niño/Southern Oscillation. *Science,* **274,** 76–78.

——, 1997a: An equatorial recharge paradigm for ENSO. Part I: Conceptual model. *J. Atmos. Sci.,* **54,** 811–829.

——, 1997b: An equatorial recharge paradigm for ENSO. Part II: A stripped-down coupled model. *J. Atmos. Sci.,* **54,** 830–847.

——, and J. D. Neelin, 1993a: Modes of interannual tropical ocean–atmosphere interaction—A unified view. Part I: Numerical results. *J. Atmos. Sci.,* **50,** 3477–3503.

——, and ——, 1993b: Modes of interannual tropical ocean–atmosphere interaction—A unified view. Part III: Analytical results in fully coupled cases. *J. Atmos. Sci.,* **50,** 3523–3540.

——, ——, and M. Ghil, 1994: El Niño on the devil's staircase: Annual subharmonic steps to chaos. *Science,* **264,** 70–72.

——, ——, and ——, 1996: El Niño/Southern Oscillation and the annual cycle: Subharmonic frequency-locking and aperiodicity. *Physica D,* **98,** 442–465.

Liu, Z., 1997: Oceanic regulation of the atmospheric Walker circulation. *Bull. Amer. Meteor. Soc.,* **78,** 407–411.

——, and B. Huang, 1997: A coupled theory of the tropical climatology: Warm pool, cold tongue, and Walker circulation. *J. Climate,* **10,** 1662–1679.

Mechoso, C. R., and Coauthors, 1995: The seasonal cycle over the tropical Pacific in coupled ocean–atmosphere general circulation models. *Mon. Wea. Rev.,* **123,** 2825–2838.

Münnich, M., M. Cane, and S. Zebiak, 1991: A study of self-excited oscillations of the tropical ocean–atmosphere system. Part II: Nonlinear cases. *J. Atmos. Sci.,* **48,** 1238–1248.

Neelin, J. D., 1991: The slow sea surface temperature mode and the fast-wave limit: Analytic theory for tropical interannual oscillations and experiments in a hybrid coupled model. *J. Atmos. Sci.,* **48,** 584–606.

——, and F.-F. Jin, 1993: Modes of interannual tropical ocean–at-

Unauthenticated | Downloaded 07/18/24 11:00 AM UTC

mosphere interaction—A unified view. Part II: Analytical results in the weak-coupling limit. *J. Atmos. Sci.,* **50,** 3504–3522.
——, and H. A. Dijkstra, 1995: Coupled ocean–atmosphere models and the tropical climatology. Part I: The dangers of flux-correction. *J. Climate,* **8,** 1325–1342.
——, M. Latif, and F.-F. Jin, 1994: Dynamics of coupled ocean–atmosphere models: The tropical problem. *Annu. Rev. Fluid Mech.,* **26,** 617–659.
Philander, S. G. H., 1990: *El Niño and the Southern Oscillation.* Academic Press, 293 pp.
——, D. Gu, D. Halpern, G. Lanbert, N.-C. Lau, T. Li, and R. C. Pacanowski, 1996: Why the ITCZ is mostly north of the equator. *J. Climate,* **9,** 2958–2972.
Schopf, P., and M. Suarez, 1988: Vacillations in a coupled ocean–atmosphere model. *J. Atmos. Sci.,* **45,** 549–566.
——, and ——, 1990: Ocean wave dynamics and the time scale of ENSO. *J. Phys. Oceanogr.,* **20,** 629–645.
Suarez, M., and P. S. Schopf, 1988: A delayed action oscillator for ENSO. *J. Atmos. Sci.,* **45,** 3283–3287.
Sun, D.-Z., and Z. Liu, 1996: Dynamic ocean–atmosphere coupling: A thermostat for the Tropics. *Science,* **272,** 1148–1150.
Tziperman, E., L. Stone, M. Cane, and H. Jarosh, 1994: El Niño chaos: Overlapping of resonances between the seasonal cycle and the Pacific ocean–atmosphere oscillator. *Science,* **264,** 72–74.
——, M. Cane, and S. Zebiak, 1995: Irregularity and locking to the seasonal cycle in an ENSO prediction model as explained by the quasi-periodicity route to chaos. *J. Atmos. Sci.,* **52,** 293–306.
Wakata, Y., and E. Sarachik, 1991: Unstable coupled atmosphere–ocean basin modes in the presence of a spatially varying basic state. *J. Atmos. Sci.,* **48,** 2060–2077.
Xie, S.-P., 1994: The maintenance of an equatorially asymmetric state in a hybrid coupled GCM. *J. Atmos. Sci.,* **51,** 2602–2612.
——, 1996: Effects of seasonal solar forcing on latitudinal asymmetry of the ITCZ. *J. Climate,* **9,** 2945–2950.
——, and S. G. H. Philander, 1994: A coupled ocean–atmosphere model of relevance to the ITCZ in the eastern Pacific. *Tellus,* **46A,** 340–350.
Zebiak, S., and M. Cane, 1987: A model El Niño-Southern Oscillation. *Mon. Wea. Rev.,* **115,** 2262–2278.

Unauthenticated | Downloaded 07/18/24 11:00 AM UTC